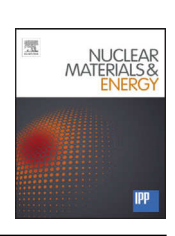
ELSEVIER

Contents lists available at ScienceDirect

Nuclear Materials and Energy

journal homepage: www.elsevier.com/locate/nme



Evaluation of the cool-down behaviour of ITER FW beryllium tiles for an early failure detection



Thomas Weber*, Andreas Bürger, Karsten Dominiczak, Gerald Pintsuk

Forschungszentrum Jülich, Institute of Energy and Climate Research, Jülich, Germany

ARTICLE INFO

Article history: Available online 9 September 2016

Keywords:
High heat flux
Cool down behaviour
Crack growth
First wall components

ABSTRACT

The design of the first wall in ITER foresees several hundred thousand beryllium tiles, which are bonded to the water-cooled CuCrZr supporting structure. Due to the nature of a Tokamak reactor this bonding is faced to thermal fatigue. Since the failure of a single tile might already have a major impact on the operability of ITER, comprehensive high heat flux tests are performed on prototypes prior to the acceptance of manufacturing procedures. For a deeper understanding of the temperature curves, which were and will be measured by IR devices of these first wall prototypes, thermo-mechanical FEM simulations shall demonstrate the possibilities of an early bonding failure detection. Hereby, the maximum temperatures for each cycle as well as the cool-down behaviour are the input data.

© 2016 The Authors. Published by Elsevier Ltd. This is an open access article under the CC BY-NC-ND license (http://creativecommons.org/licenses/by-nc-nd/4.0/).

1. Introduction

The early detection of de-bonded beryllium tiles of the first wall (FW) prototypes as a consequence of thermo-mechanical fatigue is one important aspect during their acceptance testing. Thereby, the maximum temperature of a considered tile compared to the temperature of surrounding tiles as well as the temperature development from cycle to cycle is important information for an emerging bonding damage. Surprisingly, the impact on the maximum temperature due to the presence of a crack in the joint is not that severe at high heat fluxes (2.0–2.5 MW/m²) as it is for low heat fluxes (0.5–1.0 MW/m²), meaning that enhanced temperatures are only observed at low heat fluxes, but not necessarily at high heat fluxes.

The reason for this phenomenon is a bending of the tile, coming from the temperature gradient ranging from the tile surface to the water cooling channels. The bending can actually close a gap/crack so that the thermal conductivity is restored again. Finally, while the gap impedes a thermal conduction at low heat fluxes, the thermal conductivity is restored at higher heat fluxes together with a strong bending of the tile.

But before getting to this topic in Section 2.6 some general preparative thoughts shall be shared first concerning the cool down behaviour. A quick look at a typical measured surface temperature cool down curve of actively cooled components (after the

E-mail address: tho.weber@fz-juelich.de (T. Weber).

switch off of the applied heat flux) tempts to use an exponential function for the description of the curve. Such a description could be the following formula with the initial temperature T_{max} , the coolant temperature T_{min} , the cool down constant τ , the time t and the time offset t_0 :

$$T(t) = (T_{max} - T_{min}) \cdot exp\left(-\frac{t - t_0}{\tau}\right) + T_{min}$$
(1.1)

This equation actually does not precisely fit, but still may be sufficient for the detection of a change in the cool down behaviour of a tile arising from a growing crack at the bonding. In former Tokamak experiments this approach has already been successfully implemented [1]. In Appendix A a more sophisticated semi-analytical-numerical approach is presented. Its advantage compared to Eq. (1.1) is that it stands on a physical basis: namely the heat equation. However, in view of the increased complexity, although severe simplifying assumptions are already considered, the pure numerical approach by the FEM is used in the following.

2. FEM approach

2.1. Description of the model

Viewing the difficulties induced by the temperature dependent material properties and the multi-dimensional geometry when calculating the temperature distribution analytically, the more suitable finite element method (FEM) was used to tackle this issue. For the research shown here the software ANSYS R16 was employed.

^{*} Corresponding author.

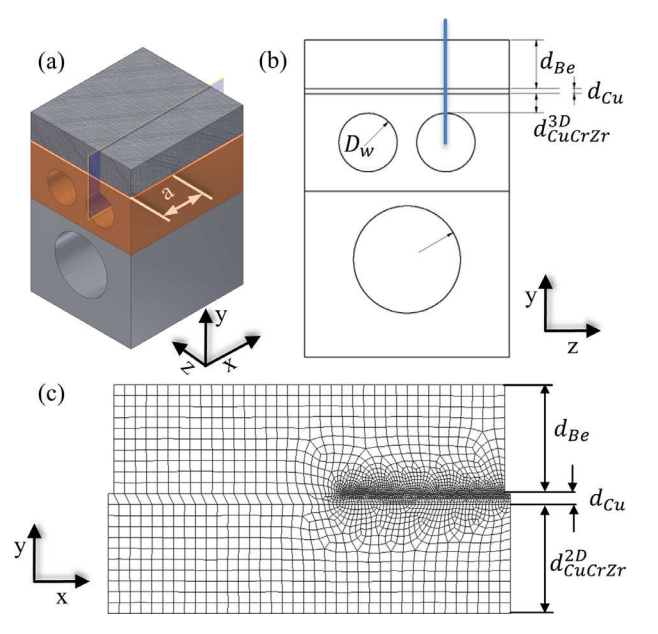


Fig. 1. (a, b) 3D and (c) 2D model of the considered part. The blue plane in (a) and (b) represents the simulated 2D region. The dense meshed region in (c) inhibits the crack between the Be tile and the Cu interlayer. (For interpretation of the references to colour in this figure legend, the reader is referred to the web version of this article.)

While in Sections 2.2 and 2.3 a comprehensive 3D model (Fig. 1 (a) and (b)) was simulated, only a 2D version in plane stress mode (Fig. 1 (c)) was used in the Sections 2.4, 2.5 and 2.6. The main reason is still the gain in computing time, so that a finer mesh and time step size can be chosen together with a larger parameter space. Thereby static structural simulations were performed using PLANE223 elements, which are capable to handle thermal and structural behaviour at the same time. The considered FW design can be found for example in [2] or [3]. Here a tube diameter D_W of 11 mm, a beryllium tile thickness d_{Be} of 10 mm, a copperinterlayer thickness d_{Cu} of 1 mm and $d_{CuCrZr}^{3D} = 6.5$ mm was used. For the 2D simulation an effective parameter $d_{CuCrZr}^{2D} = 10$ mm was used, leading to very similar temperatures as the 3D case. The tile length in x-direction was 47 mm and the width in z-direction 36 mm.

The material properties for copper, CuCrZr and beryllium were taken from [4]. They consist of density, specific heat, isotropic thermal conductivity, isotropic secant coefficient of thermal expansion, isotropic elasticity and multilinear kinematic hardening. All these properties are temperature dependant.

2.2. Thermal analysis

The following scenario is analysed regarding the impact of a present crack on the surface temperature: The top surface of the tile is loaded for 30 s at $2.0\,\mathrm{MW/m^2}$ before it cools down again for another 30 s. An initial and coolant temperature of $70\,^\circ\mathrm{C}$ and a HTC of $14\,\mathrm{kW/m^2}$ are assumed. The scenario mimics the subsequent detachment of the Be tile as a consequence of thermal-fatigue. Thereby a crack/gap with varying length a is inserted in the model between the Be tile and the Cu interlayer, so that the whole heat applied on the tile has to pass the smaller remaining intact area.

Although only one parameter set (concerning tile and interlayer thickness, heat flux intensity and duration, distance to cooling channels, etc.) is demonstrated here, the qualitative principle stays the same for other geometries. While a change in the tile width or length has a minor influence, the temperature values rise

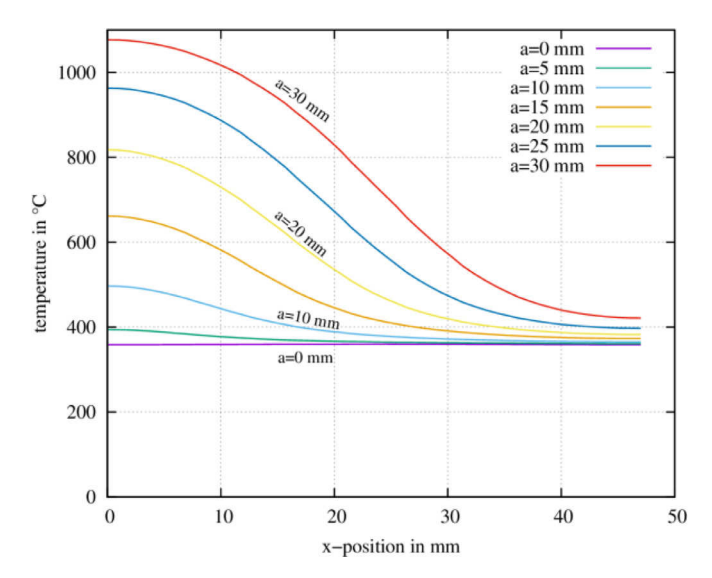


Fig. 2. Tile surface temperature distribution in dependence of the distance from the tile edge at t = 30 s for different cracks lengths a (see Fig. 1).

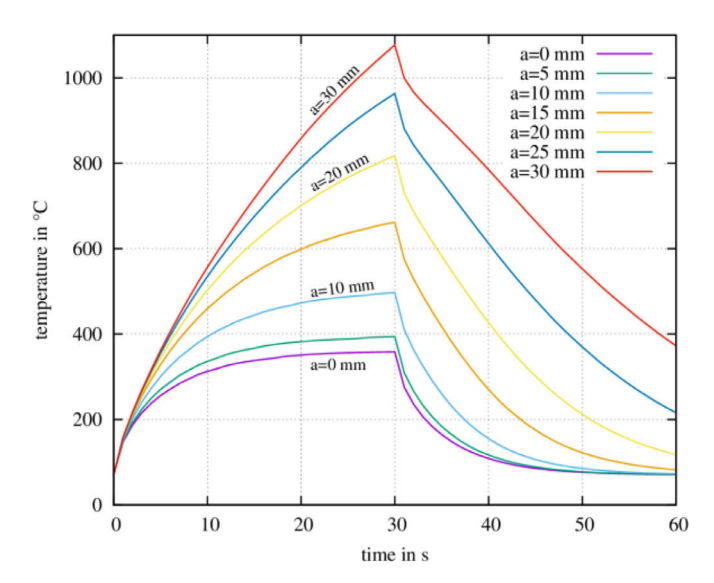


Fig. 3. Maximum temperature over time for different crack lengths $\it a$. No tile bending is considered.

with increasing distance from the cooling tube to the tile surface, namely according to the thermal conductivity of the corresponding material. The temperature difference between coolant and surface is roughly proportional to the heat flux.

The state after 30 s, when the heat flux is turned off, is shown in Fig. 2. It shows how far the influence of a crack is visible on the surface, since the spatial temperature distribution is important for the failure detection by IR cameras. Roughly half of the maximum temperature increase induced by the crack can be observed above the crack tip. As rule of thumb, for the IR image this means that the length of a hot spot is roughly twice the crack length. Assuming a noise and measuring inaccuracy of ±25 °C, hot spots can be identified when the temperature value (e.g. $T_{hot} = 385$ °C for the case shown in Fig. 3) is clearly distinguishable from the base temperature (360 °C). So the extent of a hot spot in Fig. 2 would be up to the position where the calculated temperature curves cross this threshold temperature T_{hot} . It should be mentioned that experiments at JUDITH 2 [5] always revealed hot spots caused by cracks coming from the outer edges and never were observed in the centre of a tile.

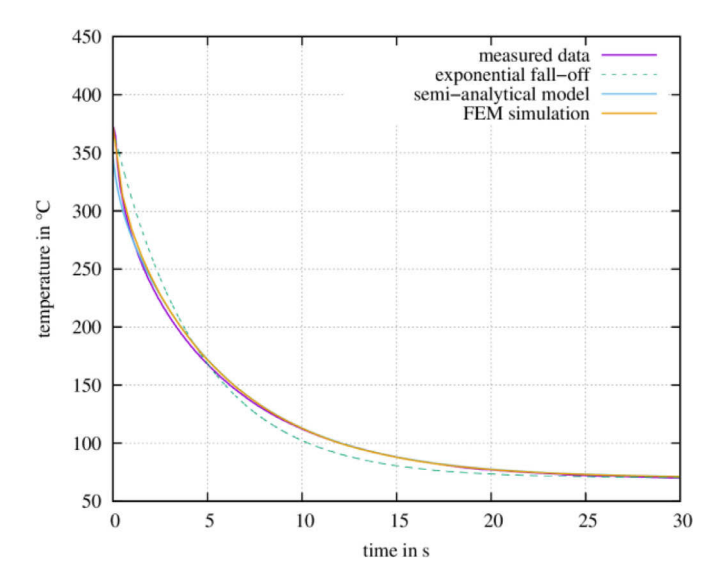


Fig. 4. Comparison of real measured data, the simple exponential fall-off function according to Eq. (1.1), the semi-analytical model according to Eq. (A.3) and the FEM-calculation (For interpretation of the references to colour in the text, the reader is referred to the web version of this article.)

The following image, Fig. 3, shows the time evolution of the maximum temperature for different crack lengths. It can be clearly seen that the maximum temperature increases as well as the cool down takes longer for growing cracks. Regarding the current considered pure thermal model this insight is not surprising at all. But things are different when the mechanical aspect is taken into account as described later on in Section 2.6.

These simple calculations allow the conclusion that, as long as the gap between the copper interlayer and the beryllium is not closed, the maximum surface temperature provides the same information about the crack length as the whole temperature cool down curve. Later on in Section 2.6 of this manuscript it will be demonstrated why the maximum temperature might be reduced when the gap is closed due to the Be tile bending.

2.3. Comparison of the models

In this subsection a short comparison between the three approaches described before is presented. Starting point is a measured cool-down curve of a beryllium tile of a tested component having the geometry shown in Fig. 1 in the JUDITH 2 facility. The applied heat flux was $\phi=2\,\text{MW/m}^2$ and the coolant temperature $T_c=70\,^{\circ}\text{C}$. This measured data is plotted as a purple line in Fig. 4.

The parameters for the exponential fall-off function (1.1) plotted as green line can easily be extracted by setting T_{max} equals to the measured temperature value at the time point of the heat flux switch-off, T_{min} equals to the coolant temperature, and finally by performing a least square fit for the determination of τ . The insight here is that such a function always overestimates the temperature in a first phase and then underestimates the temperature until the coolant temperature is reached.

For the semi-analytical model shown in Appendix A the parameter determination is more complex. Apart from the reduced number of dimensions, one instead of three, two major issues are encountered: The temperature dependence of the material properties and the number of thermal layers being limited to one. Nevertheless, the result, plotted as blue line, demonstrates that a better agreement can be achieved when appropriate parameters have been chosen. For this analysis the following values were used: $L = d_{\rm Be} + d_{\rm CCU} + d_{\rm CUCTZT}^{\rm 3D} = 17.5$ mm being the sum of the individual layers, $\lambda = 192$ $\frac{W}{m.K}$ being the effective thermal conductivity, $\alpha = 100$

 $5.05 \times 10^{-5} \,\mathrm{m^2/s}$ as effective thermal diffusivity, $h = 18.5 \,\mathrm{kW/m^2} \,\mathrm{K}$ as effective HTC, $T_{t=0}^{min} = \frac{\phi}{h} + T^c = 178 \,^{\circ}\mathrm{C}$ and $T_{t=0}^{max} = T_{t=0}^{min} + \frac{\phi \cdot l}{\lambda} = 360 \,^{\circ}\mathrm{C}$. The calculation of the effective conductivity and diffusivity for several layers of thickness l_i can be found for example in [6]:

$$\frac{L}{\lambda} = \sum_{i} \frac{l_i}{\lambda_i}$$
 and $\frac{L}{\sqrt{\alpha}} = \sum_{i} \frac{l_i}{\sqrt{\alpha_i}}$ (2.2)

Finally, the FEM simulation was performed as described in Sections 2.1 and 2.2. This model can be assumed to be the most accurate one, as long as the input material data is precise enough. In particular the measured data is often influenced by many factors leading to a deviation of up to 25 °C. This measuring error is the sum of the IR camera calibration, depositions on the mirror/glass, variations of the Be surface emissivity as a consequence of oxidation, reflected IR radiation on the Be surface, etc. In consideration of these measuring issues the very simple exponential fall-off function might be sufficient for the most purposes, because other more dedicated models with more parameters just will be disturbed by the measuring error.

2.4. Stress analysis

The analysis of the stresses and strains can be limited to the copper interlayer, since it is the only part in which plastic deformation occurs. The reason is that the yield strength of Be and Cu-CrZr are by far higher than of Cu.

So, although stresses are higher in other regions only the ones within the copper and at the interfaces are relevant. In order to consider internal residual stresses generated by the first temperature cool down after the manufacture process the initial temperature was set to 580 °C. This temperature corresponds to the joining step through hot isostatic pressing (HIP) stated in [3]. The decrease of this initial temperature from a stress free state to room temperature already induces thermal stresses. They are most intense in x-direction, being compressive inside the beryllium tile and tensile in the copper parts. A stress relief annealing is not possible in the usual sense (like it is done for parts composed of a single material), because the stresses in this joint are caused by the variation of temperature. Nevertheless, it is plausible that the stresses are actually lower when creep is taken into account. The subsequent load steps are the application of a 2 MW/m² heat flux for 30 s and a cool down for 30 s. During heating up the outer region of the copper interlayer suffers a strong compressive pressure in the y-direction by the beryllium tile, which bends itself due to the thermal gradient. At the same time the copper interlayer wants to expand itself in the x-direction, but is hindered by the beryllium, which got a smaller thermal expansion coefficient. At cool down the copper interlayer than reveals strong tensile stresses as a result of its plastic deformation during the heat up phase. For the understanding of these three stress states they are illustrated in Fig. 5. Summarised, this means that during the heating up phase no cracking occurs, because the interface stresses are compressive, but then at cool down a crack can grow because of the remaining tensile stresses in y-direction (see middle lower contour plot in Fig. 5). One should mention that only the stresses in y-direction (acting as normal force) and the shear stresses in xy-direction (acting as tangential force) contribute to the debonding of an interface, while stresses in x-direction inside the involved materials are irrelevant for the cohesion of the joint. Based hereon a qualitative analysis on the crack growth mechanism is presented in the following section.

2.5. Crack growth analysis

Fracture mechanics can be split into linear elastic fracture mechanics (LEFM) and into elastic-plastic fracture mechanics (EPFM).

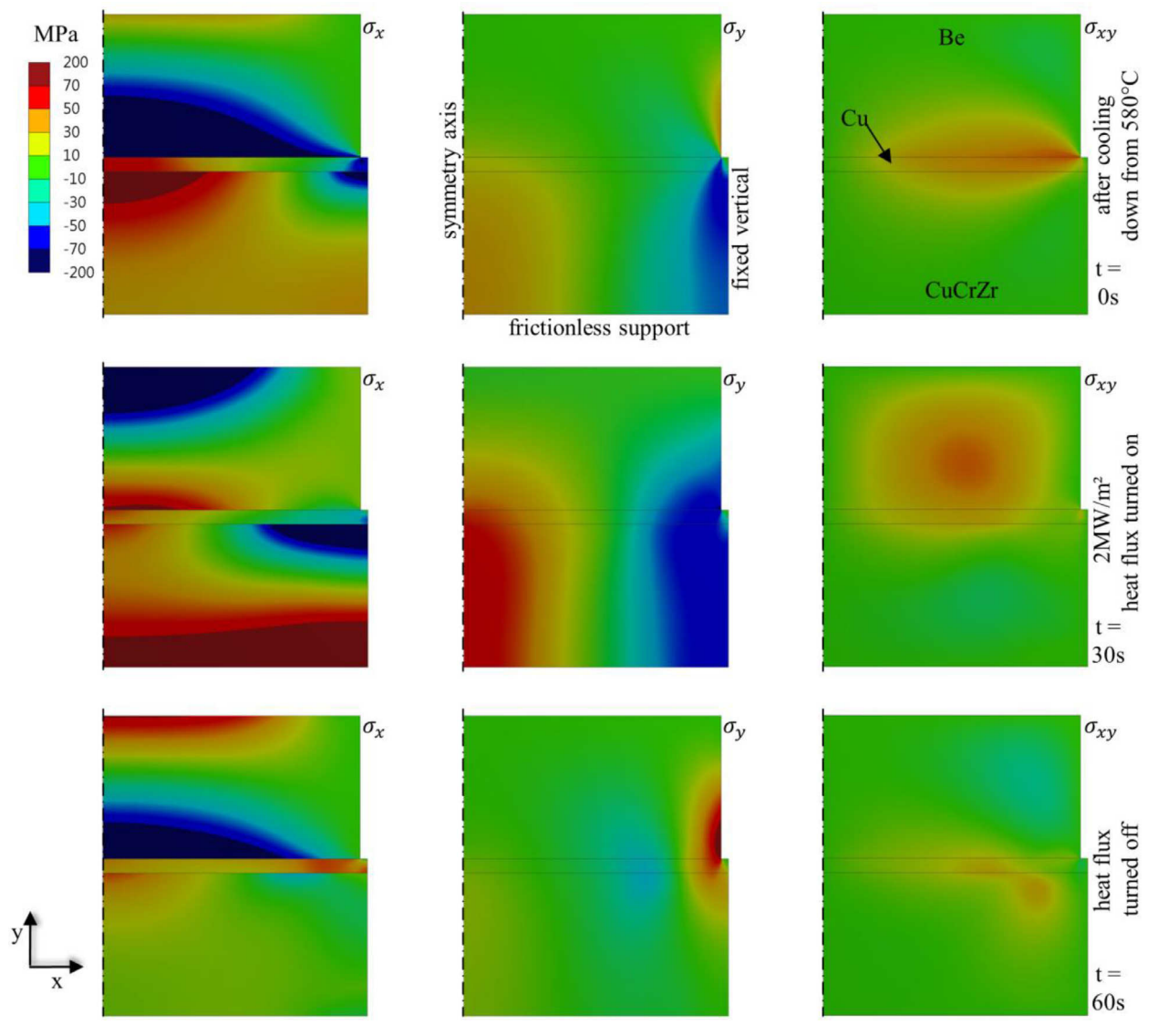


Fig. 5. Stress states at t = 0 s (upper row), t = 30 s (mid row) and t = 60 s (lower row).

Table 1 Material properties used for the bonding between Be and Cu.

Parameter	Value	Unit
Maximum normal contact stress	90	MPa
Contact gap at complete debonding	0.001	Mm
Max. equiv. tangential contact stress	90	MPa
Tangential slip at complete debonding	0.001	Mm
Artificial damping coefficient	0.0001	s

In FEM the two common parameters, the stress intensity factor (LEFM) and the J-integral (EPFM), can be easily extracted by today's ANSYS version. For the considered model here the purely elastic approach is inadequate, since the plastic deformation of the stress relieving copper interlayer needs to be taken into account. The J-integral is actually the most adequate method, but because of its complexity a third, simpler and still sufficient, approach is applied: the cohesive zone model (CZM). Along the different variants implemented in ANSYS a separation-distance based debonding was used at mixed interface mode with tangential slip under normal compression turned on. The corresponding properties of the bond are listed in Table 1. At this point it has to be clearly said, that

the assumed bonding strength is purely fictive. A higher strength would cause a decrease of the crack growth per cycle, while a lower value would have the contrary consequence. The reason for this rough assumption, which is not based on measured material data, is (apart from not being known to the authors) that the aim here is not the estimation of lifetime. Much more the geometrical shape and consequence of a present crack on the temperature distribution is subject of this investigation. The lifetime estimation would have to consider the fatigue of the copper interlayer and its reduction in stiffness as well as stress assisted oxidation effects of the crack surface and even neutron embrittlement. Experiments at JUDITH 2 showed that the crack growth can last several thousand cycles, but also can occur within a few tenth thermal cycles. A spontaneous failure within one single cycle, leading to a complete detachment of the tile, can occur if the bonding at the tile centre is faulty. In such a case the stress in y-direction during the heat loading phase shown in Fig. 5 leads to unstable crack propagation.

The heat radiation between both crack surfaces is negligible at such low temperatures compared to the heat flux applied by the fusion plasma. Also convection can be neglected at vacuum conditions.

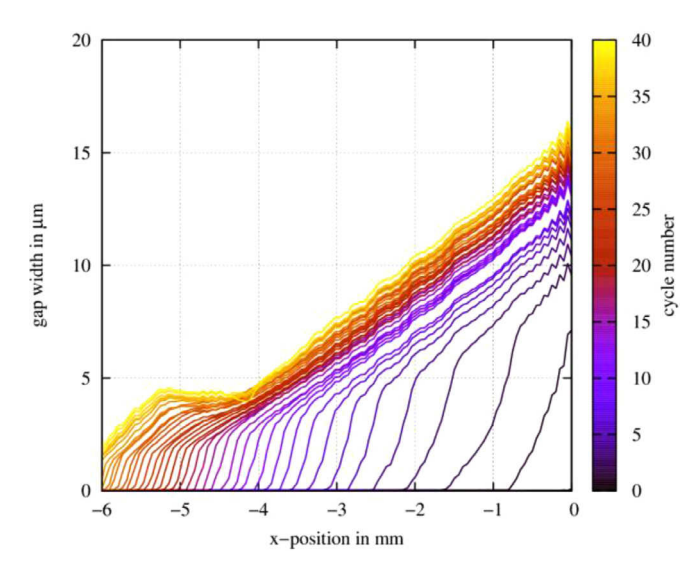


Fig. 6. Gap width over x-position for each cycle. x = 0 is located at the right border of the Be tile.

The geometry of the crack, which grows from cycle to cycle is shown in Figs. 6 and 7. During the heating up phase no cracking occurs, because the interface stresses are compressive, but then at cool down a crack can growth because of the remaining tensile stresses.

2.6. Influence of tile bending on temperature

In this final section the influence of the crack closure through the tile bending on the cool down behaviour shall be shown in a qualitative manner. Due to severe convergence issues of the solving algorithm, plasticity was turned off in the simulations presented in this last section. Since plasticity is essential for the crack growing mechanism, as shown in Section 2.5, an initial crack of certain length was assumed. Based on Fig. 6 a triangular shaped crack was inserted in the initial state. Thereby the Be tile was kept untouched, while copper material was removed such that a triangle, having a slope of $2.5\,\mu\text{m/mm}$, was missing. In principle like the white triangle in the most right image in Fig. 7, but extrapolated for greater crack lengths. Of course, in the real situation no material is removed, instead it is pressed outwards cycle by cycle. The slope was selected according to the gap width of $15\,\mu\text{m}$ for a crack length of $6\,\text{mm}$ (Fig. 6) and is characteristic for

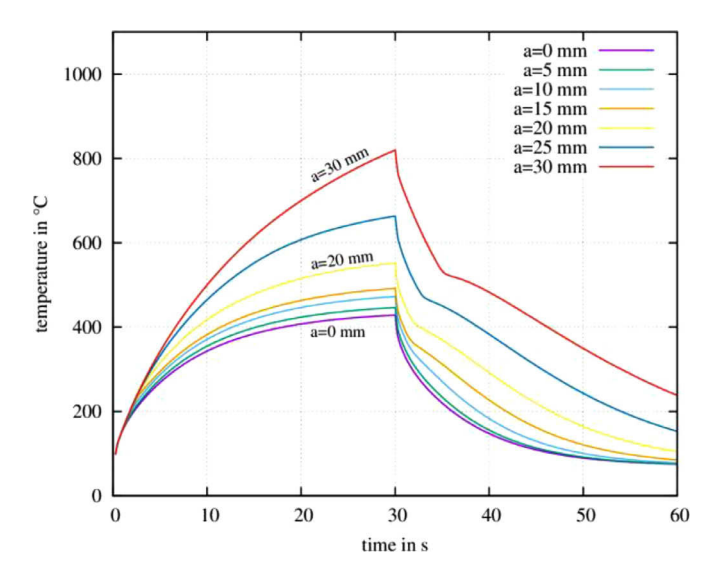


Fig. 8. Maximum temperature over time for different crack lengths a. Tile bending is considered.

a crack grown at 2.0 MW/m². Other heat fluxes would also yield other slopes. For sure there is still a certain uncertainty concerning the exact crack shape, because it is extrapolated from 6 to 30 mm crack length. Experimental cross-section cuts are unfortunately not available for verification, but for the purpose of temperature calculation followed here this assumption is sufficient. Thermal conductivity was restored to a thermal contact conductance coefficient of $20 \, \text{kW/m}^2 \, \text{K}$ as soon as the gap width was smaller than $2 \, \mu \text{m}$. Such a coefficient value is realistic for metals of different kinds and in particular for copper [7–9]. A more dedicated model should actually consider the pressure dependence of the thermal conductivity between two surfaces. However, since this experimental data is not available yet, the numerically simpler gap dependent approach was used.

Finally, the maximum temperature and the cool down constant τ are both plotted over the crack length in Figs. 9 and 10, respectively. Therefore the function (1.1) was fitted on the cool down curves shown in Figs. 3 and 8. It reveals that the constant τ is indeed more meaningful than the maximum temperature.

The two parameters τ and T_{max} were calculated for several crack lengths ranging from 0 to 30 mm and heat fluxes (0.5, 1.0 and 2.0 MW/m²). Since the gap cannot be closed if the heat flux is too low, e.g. 0.5 MW/m², there is no difference on the maximum

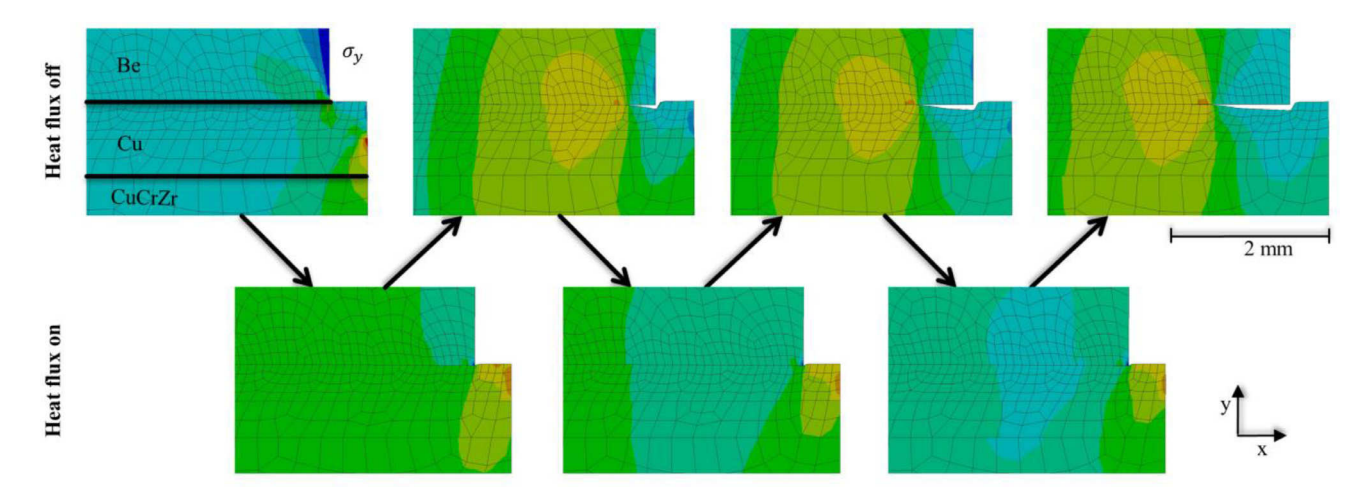


Fig. 7. Stress in y-direction for the first three thermal cycles demonstrating the crack growth mechanism. Deformations are scaled by a factor of 100.

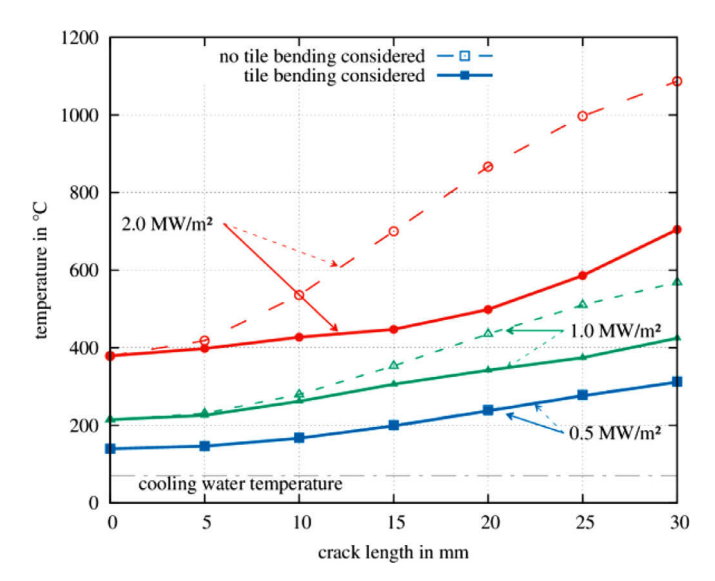


Fig. 9. Maximum surface temperature over crack length at different heat fluxes with and without consideration of the tile bending.

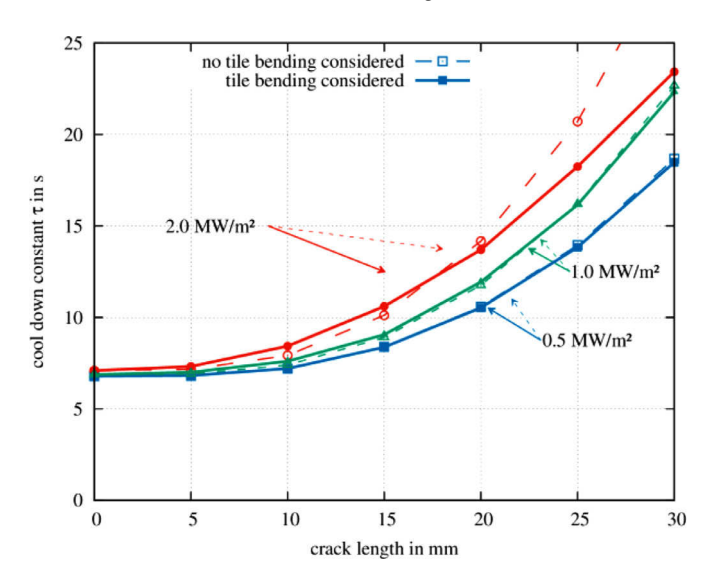


Fig. 10. Cool down constant τ over crack length at different heat fluxes with and without consideration of the tile bending.

temperature between the situation where tile bending is considered and not considered. Now, as soon as the heat flux is high enough to cause a temperature gradient steep enough, so that the beryllium tile is bended so strong, that the gap is closed again, the maximum temperature can be strongly reduced.

3. Conclusion

This theoretical work presented here built the basis for the understanding of experimentally observed effects. Evaluating only the maximum temperature, what is a sufficient method when no recovery of the thermal conductivity across a crack occurs, can actually become unfruitful due to the tile bending. Instead, the evaluation of the cool down constant τ is successful what is clearly shown in Fig. 10. The reason is that the crack closure occurs shortly after the heat flux is switch on, but the crack opens again shortly after the heat flux is switched off.

In principle these insights are not limited to high heat flux testing. They also help to understand the measured temperatures of the FW in ITER, but certain assumptions used here are not fulfilled

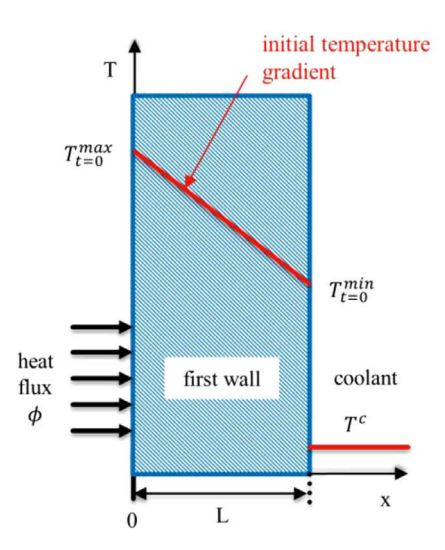


Fig. 11. Analytical 1D model showing the considered geometry and initial state.

and need to be considered in a more sophisticated way. For example the thermal power during the shutdown procedure of the fusion reactor does not fall off instantly to zero. Instead, a smooth fall off can be expected. Also the heterogeneous heat flux distribution and glancing observation angle complicates an evaluation. Finally, for practical reasons the use of the fitting function (1.1) is actually a good choice, considering the vast effort necessary for other approaches.

Appendix A. Semi-analytical approach

To ease up the situation only a 1D model, having a certain heat flux on one side, a thermally conducting layer and convection to a coolant on the other side, is considered (Fig. 11). Starting point of such a model is the heat equation

$$\frac{\partial T(x,t)}{\partial x^2} = \frac{1}{\alpha} \frac{\partial T(x,t)}{\partial t}$$
 (A.3)

with the temperature T(x, t) at time t and position x and the thermal diffusivity $\alpha = \frac{\lambda}{c_p \cdot \rho}$ composed by the thermal conductivity λ , the density ρ and the specific heat capacity c_p .

Depending on the choice of initial state and boundary conditions of the function T(x, t) either the loaded or unloaded scenario can be formulated. While the 1D temperature distribution of the first wall being loaded by a constant heat flux at thermal equilibrium state is easily analytically calculable, the calculation of the cool down temperature in the unloaded state is not. Since the solution of the first case is a simple linear temperature gradient, which serves as initial state for the second case, no further attention is paid on it. The unloaded scenario is described as follows: The heat transfer coefficient (HTC) $h_{x=0}$ at the surface of the first wall is set to zero resulting into perfect thermal insulation. So no radiation or convection is taken into account. On the coolant side a HTC of $h_{x=L} = h$ is considered. This is expressed in the boundary conditions:

$$-\lambda \frac{\partial T(x,t)}{\partial x} + h_{x=0} \cdot T(x,t) = 0 \quad \text{at} \quad x = 0$$

$$\lambda \frac{\partial T(x,t)}{\partial x} + h_{x=L} \cdot T(x,t) = 0 \quad \text{at} \quad x = L$$
(A.4)

These boundary conditions imply a coolant temperature T^c of zero. To consider a non-zero coolant temperature T^c it must be subtracted from the initial state temperature and then added afterwards to the result temperature T(x, t). The initial state is given as linear temperature gradient between x = 0 and x = L being the

steady state situation under heat flux loading, which is illustrated in Fig. 11.

$$T(x,0) = T_{t=0}^{max} - \frac{T_{t=0}^{max} - T_{t=0}^{min}}{L} x - T^{c}$$
(A.5)

While the coolant temperature T^c and the heat flux density ϕ are given, the steady state temperature at the inner wall is $T_{t=0}^{min} = \frac{\phi}{h} + T^c$ and the temperature of the surface facing the heat flux is $T_{t=0}^{max} = T_{t=0}^{min} + \frac{\phi \cdot L}{r}$.

 $T_{t=0}^{max} = T_{t=0}^{min} + \frac{\phi \cdot L}{\lambda}$.

A solution can be gained by separation of variables using the following solution approach shown in [10]:

$$T(x,t) = \sum_{m=1}^{\infty} c_m \cdot \cos(\beta_m x) \cdot exp(-\alpha \cdot \beta_m^2 \cdot t)$$
 (A.6)

Thereby the coefficients c_m of the Eigenfunctions are

$$c_m = \frac{1}{N(\beta_m)} \int_0^L \cos(\beta_m x) \cdot T(x, 0) \cdot dx \tag{A.7}$$

with the norm

$$N(\beta_m) = \frac{2\beta_m L + \sin(2\beta_m L)}{4\beta_m}$$
 (A.8)

However, the coefficients β_m still must be calculated numerically by solving the equation

$$\cot\left(\beta_{m}L\right) = \frac{\beta_{m}\lambda}{h}.\tag{A.9}$$

This analytical model describes a flat plate cooled by any coolant via the parameters L, λ , ρ , c_p , $T_{t=0}^{min}$, $T_{t=0}^{max}$ and h. A more sophisticated model actually should also consider the cooling tube

geometry and the temperature dependence of the material properties: $\lambda(T)$, $\rho(T)$ and $c_p(T)$. Unfortunately, 2D or even 3D coupled inhomogeneous time dependent equations with such boundary conditions cannot be solved purely analytical. A work-around for the geometry issue could be implemented by using 'effective' parameters, but the temperature dependence is insurmountable. This issue leads to the next approach followed in Section 2.

References

- R. Mitteau, J. Schlosser, M. Lipa, A. Durocher, Power operation with reduced heat transmitting tiles at tore supra, J. Nucl. Mater. 386–388 (2009) 844–846.
- [2] T. Cicero, et al., Progress in the design of Normal Heat Flux First Wall panels for ITER, Fusion Eng. Des. 98–99 (2015) 1256–1262.
- [3] S. Banetta, F. Zacchia, P. Lorenzetto, I. Bobin-Vastra, B. Boireau, A. Cottin, R. Mitteau, R. Eaton, R. Raffray, Manufacturing of small-scale mock-ups and of a semi-prototype of the ITER Normal Heat Flux First Wall, Fusion Eng. Des. 89 (2014) 970–974
- [4] ITER, Structural design criteria for ITER in-vessel components (SDC-IC, Appendix A, Materials design limit data), (2011), ITER Doc. G 74 MA 8 01-05-28 W0 2
- [5] P. Majerus, R. Duwe, T. Hirai, W. Kühnlein, J. Linke, M. Rödig, The new electron beam test facility JUDITH II for high heat flux experiments on plasma facing components, Fusion Eng. Des. 75–79 (2005) 365–369.
- [6] G. Gonzalez de la Cruz, Yu.G. Gurevich, Thermal diffusion of a two-layer system, Phys. Rev. B 51 (4)) (1995) 2188–2192.
- [7] H.L. Atkins, Thermal contact conductance in a vacuum, 1965 Technical Report (MIT, Heat Transfer Laboratory), No. 39.
- [8] A.KJ. Hasselström, U.E. Nilsson, Thermal Contact Conductance in Bolted Joints, Charlmers University of Technology, Gothenburg, 2015 Diploma work.
- [9] C. Ma, L. Zhao, H. Shi, X. Mei, J. Yang, A geometrical-mechanical-thermal predictive model for thermal contact conductance in vacuum environment, Proc. Inst. Mech. Eng., Part B: J. Eng. Manuf. (2015) 1–14, doi:10.1177/ 0954405415611358.
- [10] Lecture 'conduction heat transfer' of Professor Ernesto Gutierrez-Miravete, Rensselaer Polytechnic Institute. Chapter 5. Section 4.2. (2006).